Preventing oil spills:

How spintronics will change the game

Alena Boyko
SURE 2019
Supervisor: Prof. Gang Xiao,
Brown University

Quick facts on oil-related accidents

- In the United States, from 1971 through 2000, the Coast Guard recorded over **250,000** oil spills in U.S. Waters.
- The largest oil spill in US history (2010, Gulf of Mexico), brought about: **200 millions** gallons of oil spilt, **$56 billion** of fines and costs, **11** people dead, **17** injured, **thousands** of animals dead.
- Among the causes of the catastrophe, experts name **concrete integrity issues** and **late identification** of the problem

Picture credit: "Damaged or Cracked Wellbore Animation | 3D Drilling Animation | Downhole Animation" https://www.youtube.com/watch?v=qwkJd_cQ0UE
'Learn from the past: Deepwater Horizon oil spill" https://safety4sea.com/cm-learn-from-the-past-deepwater-horizon-oil-spill/

KAUST proposal

Parameters of the model:

- Desired frequency range of 1-10 kHz
- Temperature in the wellbore goes up to 100 ∘C, heat insulation will be required to protect the electronics
- Original paper assumes a large transmitter coil and high relative permeability of concrete (up to 2)
- Design is not suitable for MTJ’s use: signal will be too small, we plan to use a gradiometer instead

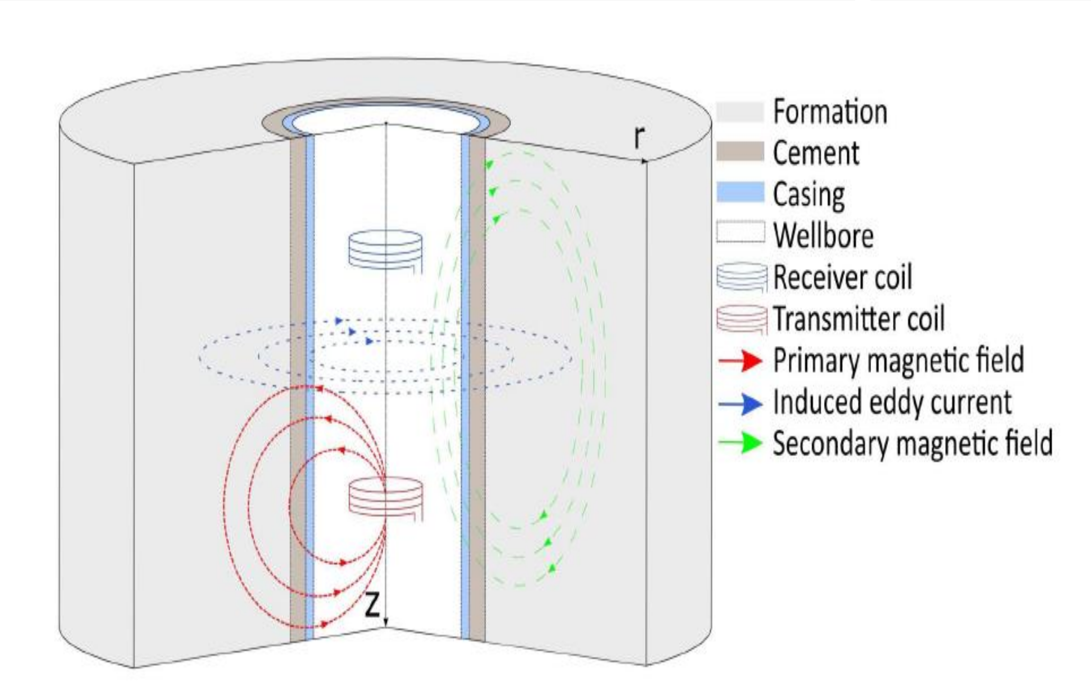

Fig. 1. A model of wellbore (by Timofey Eltsov)

Parameter	Wellbore	Fiberglass	Concrete	Formation
Radius, m	0.07	0.1	0.15	
Resistivity, Ω·m	2	10^8	100	50
Magnetic permeability	1	1	1 - 2	1

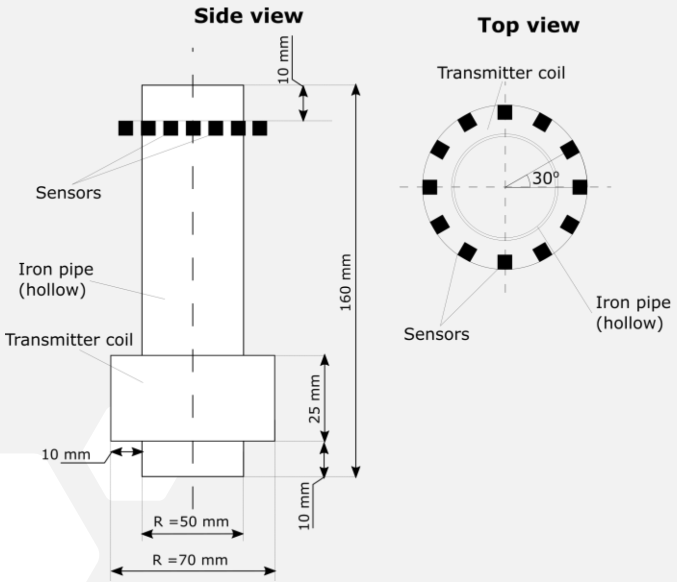

Fig. 2. The original design (by Timofey Eltsov)

MTJ – Magnetic Tunnel Junction

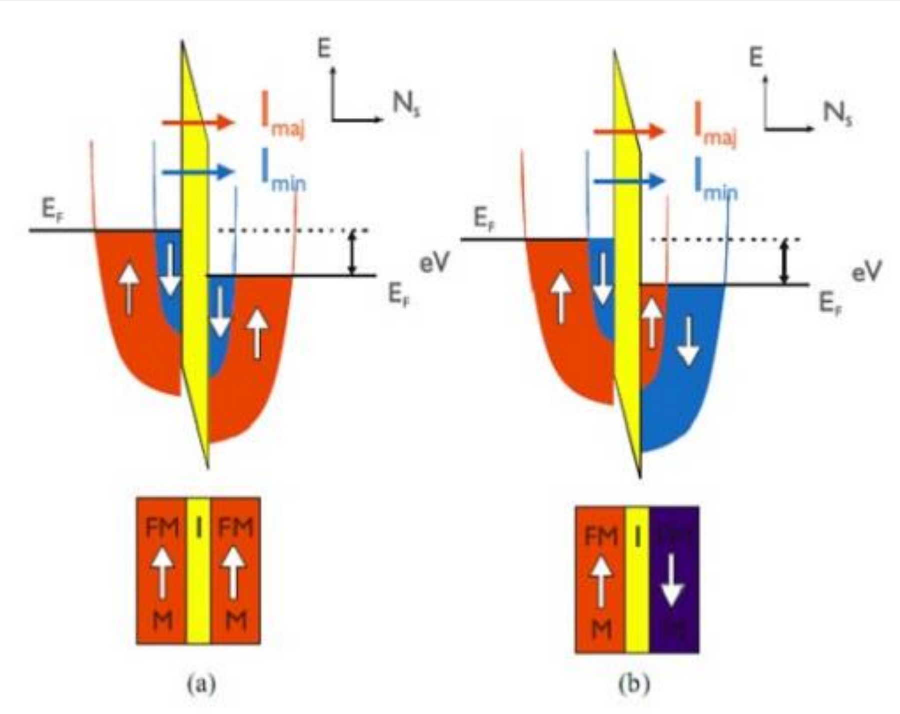

In a magnetic tunneling junction, the density of states of both plates determines whether a large current (a) or small current (b) tunnels through.

Fig. 3. Spin-dependent tunneling

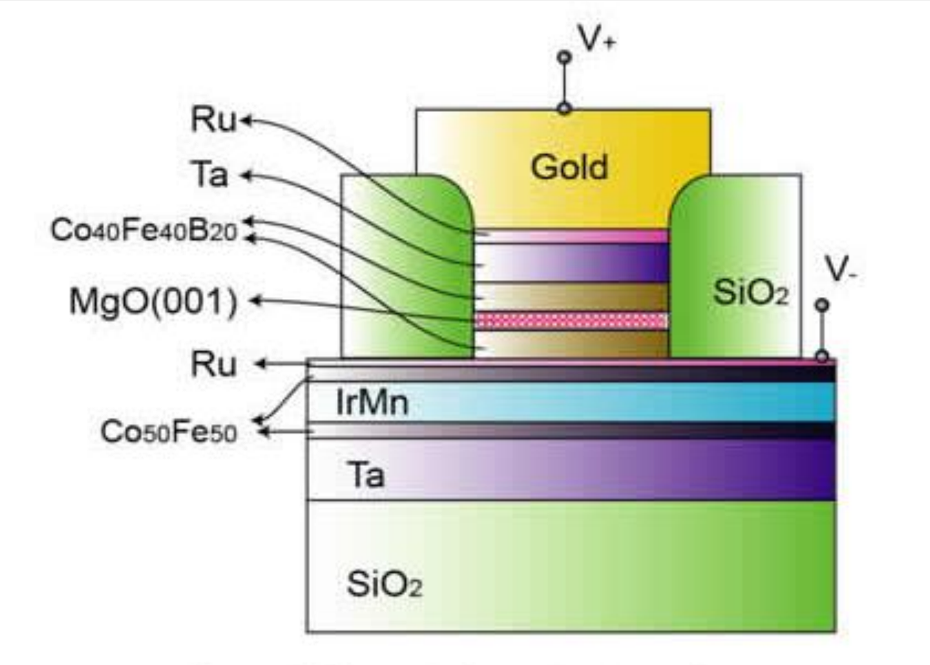

Figure 1: Schematic layer structure of an MgO-based magnetic tunnel junction sensor

Fig. 4. A typical MTJ structure

Picture credit: https://www.brown.edu/research/labs/xiao, courtesy of Prof. Xiao

Part I: Simulation

2D simulation (COMSOL)

Geometrical sizes were preserved from the original proposal

Materials: granite, concrete (relative magnetic permeability 1.02), fiberglass, oil (to replace drilling mud), air

Distance from the probes to the fiberglass: 1 cm

Field source: magnetic point dipole 0.01 A·m^2

DC mode used to save time

2 configurations tested, parallel and perpendicular to the surface (parametric sweep of the position of the cavity)

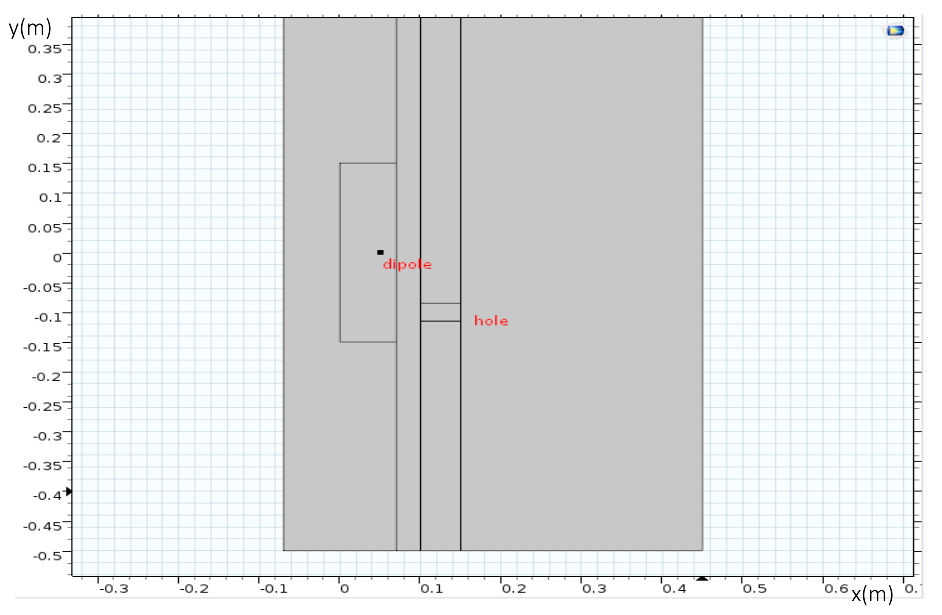

Fig. 5. The 2D model of a wellbore

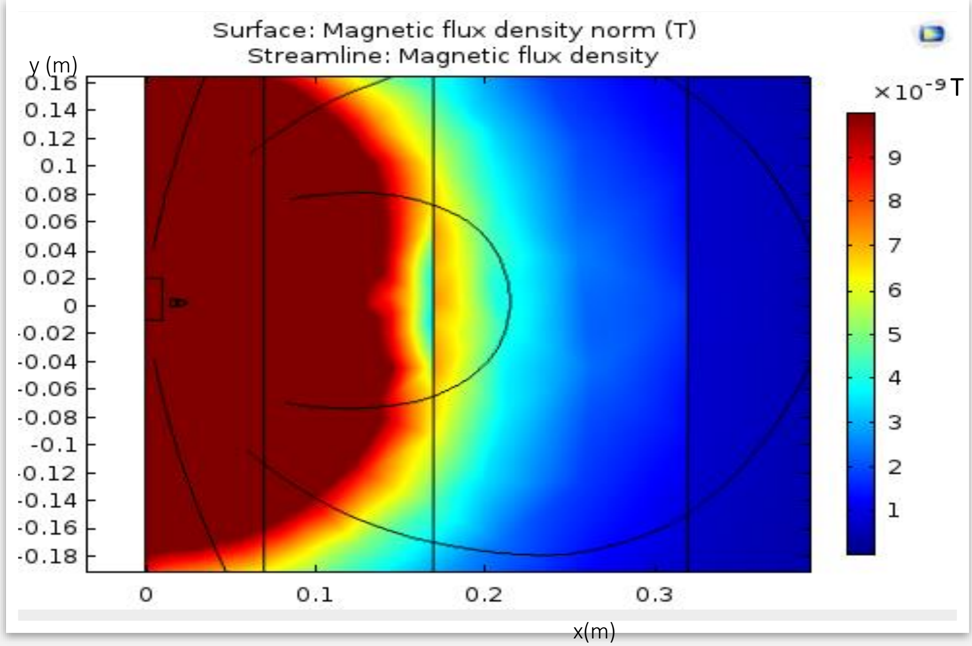

Fig. 6. Simulated magnetic response of the concrete

Signal (2D results)

- pT range of the signal – can be resolved by using stronger coil field
- Simulation results demonstrate a constant offset of the signal (removed here), 2-3 orders of magnitude greater than the signal itself

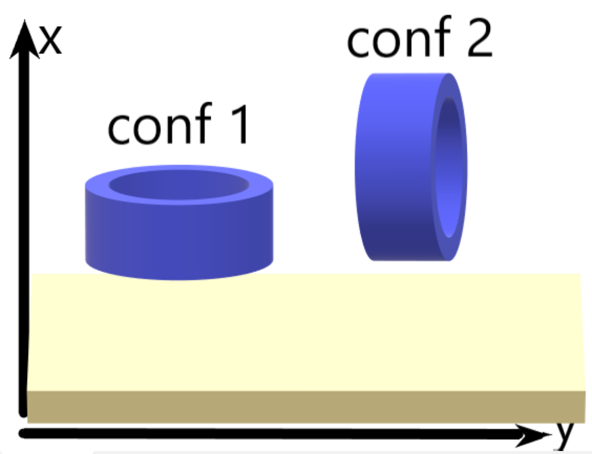

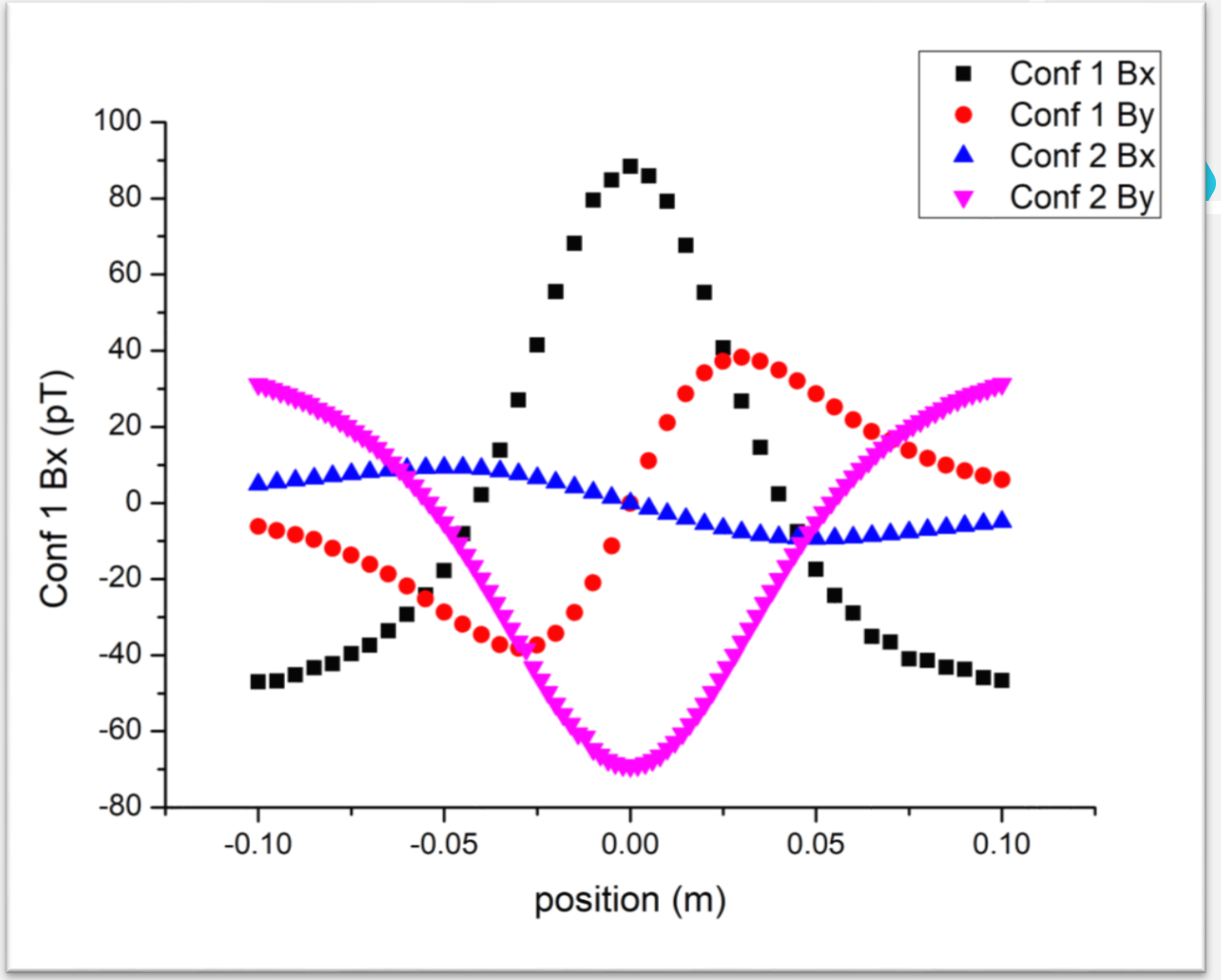

Fig. 7. The predicted gradiometer signal (adjusted)

Part II: Experiment

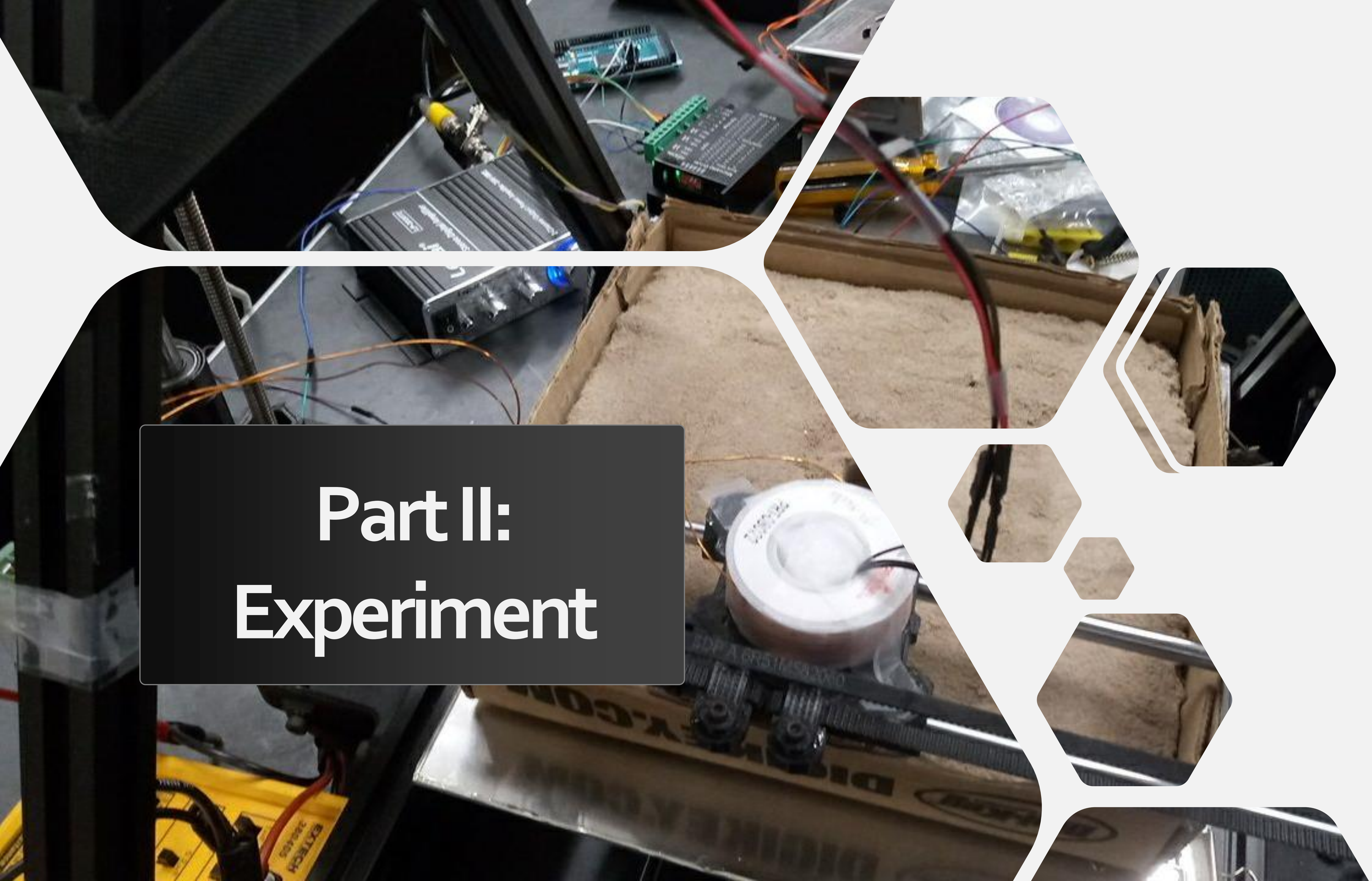

Magnetic sand

Limitations and issues:

- Non-uniform mixing – sand grain size varies and a light shaking of the box will cause iron powder to slide downwards – switched to using gypsum powder instead of sand to build a solid piece of "concrete"
- Desired upper limit on the iron amount – 3 % by mass
- Steel powder magnetization turned out to be weaker than that for the bulk iron

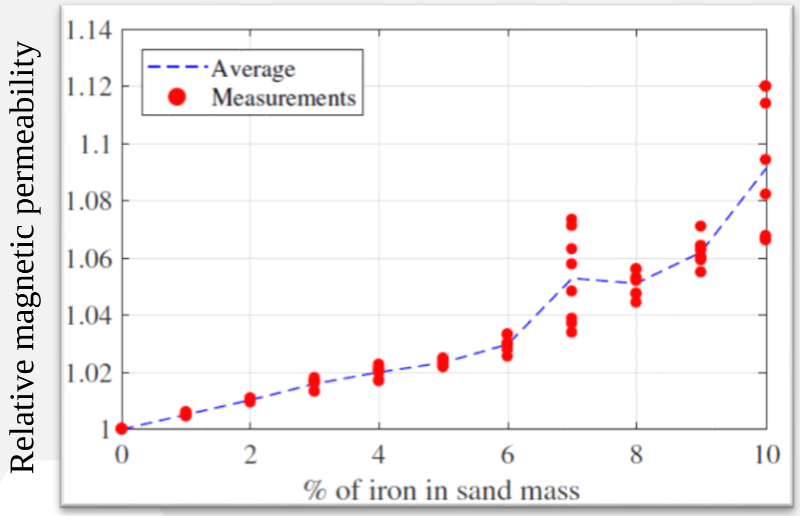

Fig. 8. Measured relative permeability of concrete (performed by KAUST group)

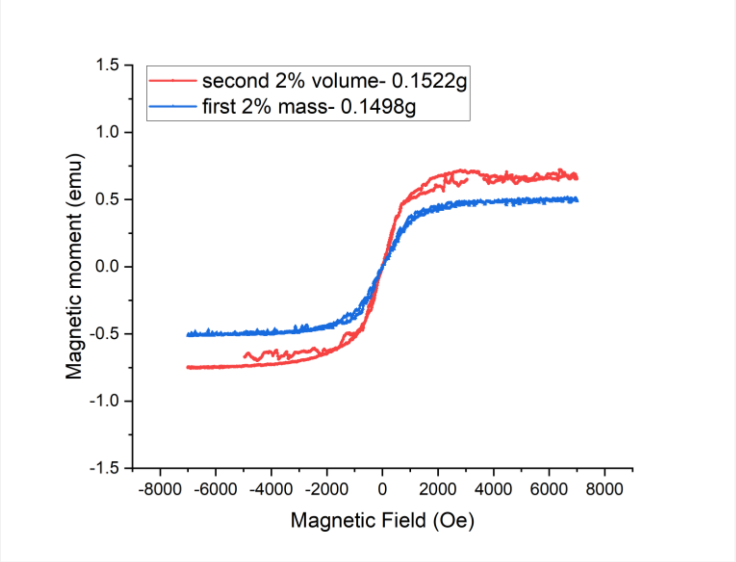

Fig. 9. Measured magnetizations of mixtures

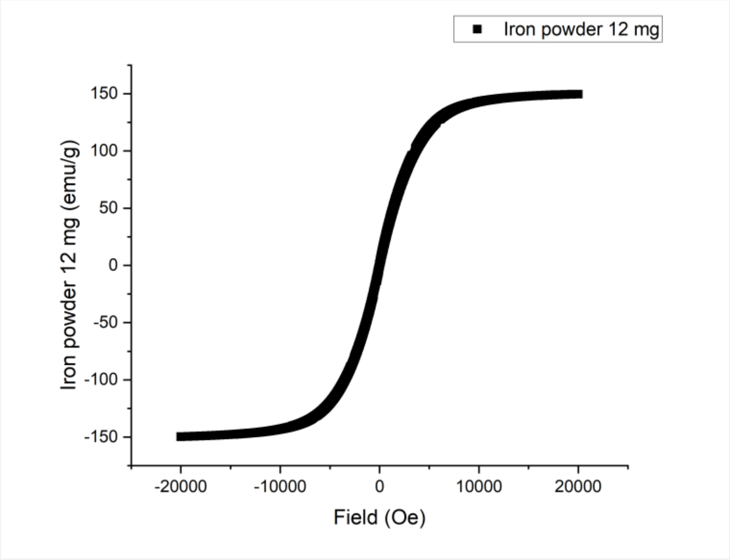

Fig. 10. Measured magnetization of iron powder

Density of sand: 1,75 g/cm^3
Density of iron powder: 3,59 g/cm^3

Saturation magnetization measurements results:

2% mass measurement:

- Predicted: 0.44 emu
- Measured: 0.5 emu (+13% error)

2% volume measurement (porosity effects not included)

- Predicted: 0.9 emu
- Measured: 0,7 emu (-23% error)

- Non-uniform mixing
- Cavities contributions

Examples of the issues with concrete modelling

Helmholtz coil calibration

- Satisfactory but not ideal field of the coil itself
- Uniform field is not truly uniform and sensor can easily detect it -> cannot minimize CMR ratio well

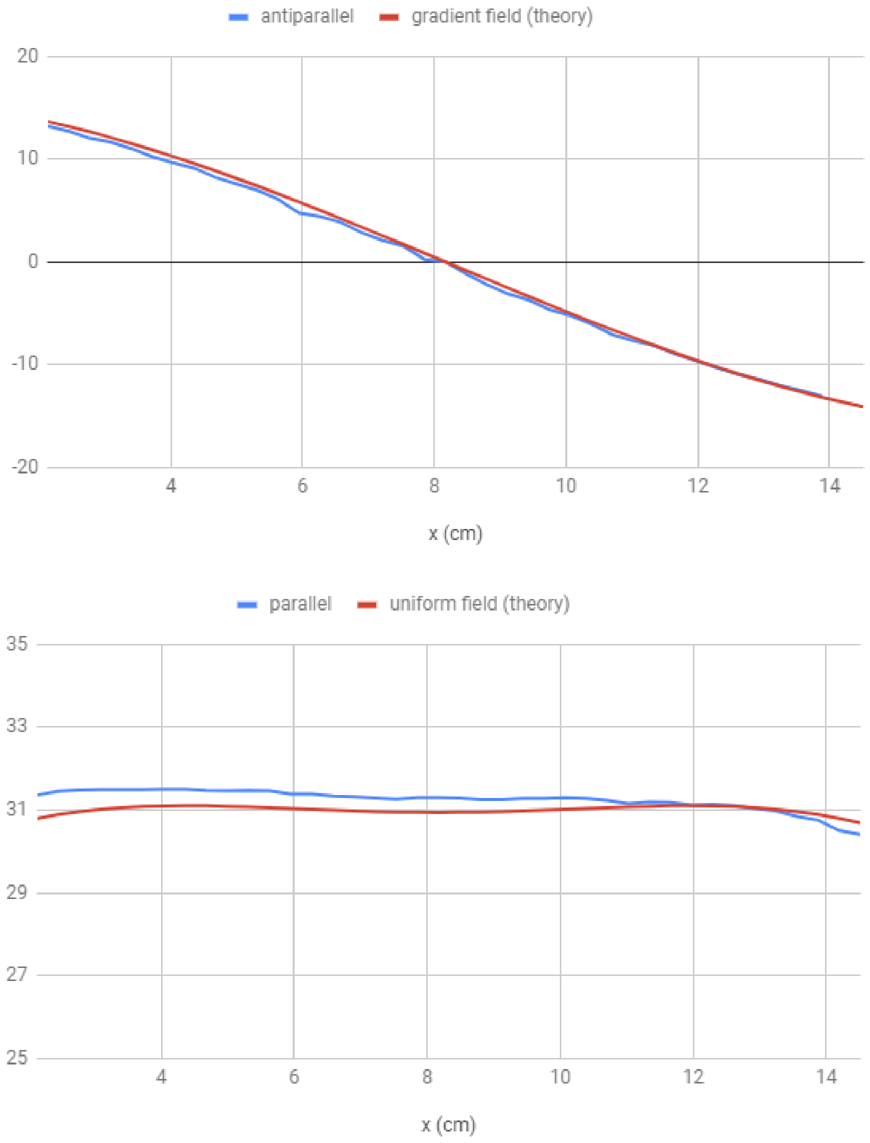

Fig. 11. Helmholtz coil calibration

Sensor calibration

- Inconsistent
- The output might be dependent on the field to some extent
- Uniform-field fit seems to be more consistent
- Unexplained dip in the middle of gradient field curve
- Saturation field of MTJ limits the use of the coil potential

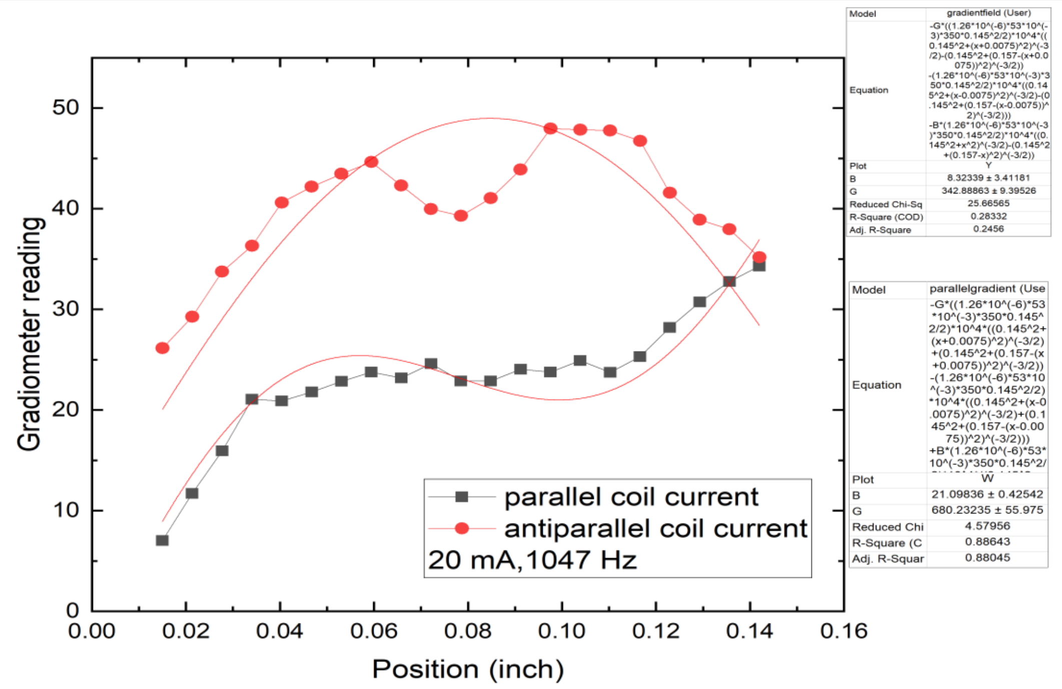

Model	gradientfield (User)
Equation	-G*((1.26*10^(-6)*53*10^(-3)*350*0.145^2/2)*10^4*((0.145^2+(x+0.0075)^2)^(-3/2)-(0.145^2+(0.157-(x+0.0075))^2)^(-3/2)) -(1.26*10^(-6)*53*10^(-3)*350*0.145^2/2)*10^4*((0.145^2+(x-0.0075)^2)^(-3/2)-(0.145^2+(0.157-(x-0.0075))^2)^(-3/2))) -B*(1.26*10^(-6)*53*10^(-3)*350*0.145^2/2)*10^4*((0.145^2+x^2)^(-3/2)-(0.145^2+(0.157-x)^2)^(-3/2))
Plot	Y
B	8.32339 ± 3.41181
G	342.88863 ± 9.39526
Reduced Chi-Sq	25.66565
R-Square (COD)	0.28332
Adj. R-Square	0.2456

Model	parallelgradient (Use
Equation	-G*((1.26*10^(-6)*53*10^(-3)*350*0.145^2/2)*10^4*((0.145^2+(x+0.0075)^2)^(-3/2)+(0.145^2+(0.157-(x+0.0075))^2)^(-3/2)) -(1.26*10^(-6)*53*10^(-3)*350*0.145^2/2)*10^4*((0.145^2+(x-0.0075)^2)^(-3/2)+(0.145^2+(0.157-(x-0.0075))^2)^(-3/2))) +B*(1.26*10^(-6)*53*10^(-3)*350*0.145^2/
Plot	W
B	21.09836 ± 0.42542
G	680.23235 ± 55.975
Reduced Chi	4.57956
R-Square (C	0.88643
Adj. R-Squar	0.88045

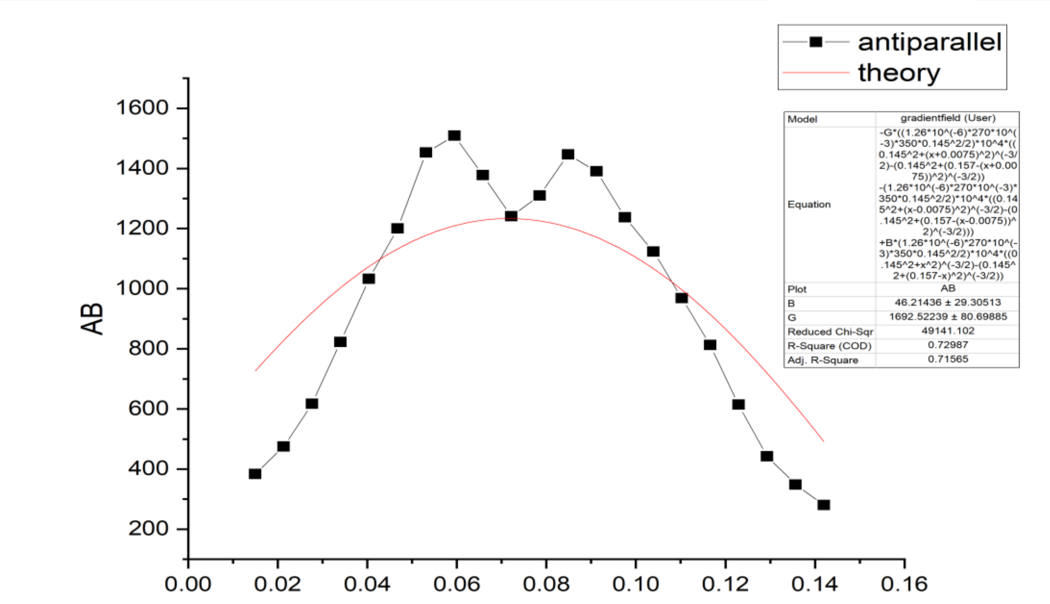

Model	gradientfield (User)
Equation	-G*((1.26*10^(-6)*270*10^(-3)*350*0.145^2/2)*10^4*((0.145^2+(x+0.0075)^2)^(-3/2)-(0.145^2+(0.157-(x+0.0075))^2)^(-3/2)) -(1.26*10^(-6)*270*10^(-3)*350*0.145^2/2)*10^4*((0.145^2+(x-0.0075)^2)^(-3/2)-(0.145^2+(0.157-(x-0.0075))^2)^(-3/2))) +B*(1.26*10^(-6)*270*10^(-3)*350*0.145^2/2)*10^4*((0.145^2+x^2)^(-3/2)-(0.145^2+(0.157-x)^2)^(-3/2))
Plot	AB
B	46.21436 ± 29.30513
G	1692.52239 ± 80.69885
Reduced Chi-Sqr	49141.102
R-Square (COD)	0.72987
Adj. R-Square	0.71565

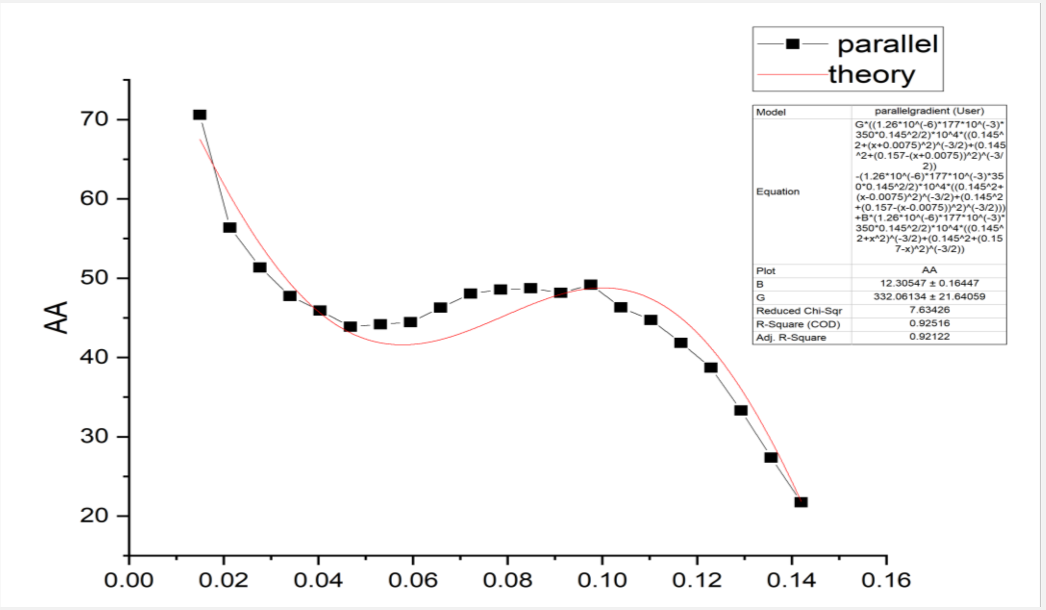

Model	parallelgradient (User)
Equation	G*((1.26*10^(-6)*177*10^(-3)*350*0.145^2/2)*10^4*((0.145^2+(x+0.0075)^2)^(-3/2)+(0.145^2+(0.157-(x+0.0075))^2)^(-3/2)) -(1.26*10^(-6)*177*10^(-3)*350*0.145^2/2)*10^4*((0.145^2+(x-0.0075)^2)^(-3/2)+(0.145^2+(0.157-(x-0.0075))^2)^(-3/2))) +B*(1.26*10^(-6)*177*10^(-3)*350*0.145^2/2)*10^4*((0.145^2+x^2)^(-3/2)+(0.145^2+(0.157-x)^2)^(-3/2))
Plot	AA
B	12.30547 ± 0.16447
G	332.06134 ± 21.64059
Reduced Chi-Sqr	7.63426
R-Square (COD)	0.92516
Adj. R-Square	0.92122

Fig. 12. Helmholtz coil calibration attempts

Field of the coil

The coil used currently:

200 turns, radius 2 cm, AWG 21 (allows current up to 1.2 A)

Maximum magnetic moment 0.3 A·m^2 (DC field up to 55+ G)

KEPCO power supply can be very useful for getting large DC current, but does not give out large AC current when connected to the signal generator; we've used small audio amplifier instead and a box of capacitors to reach the resonance (the inductance of small coil is around 3 mH)

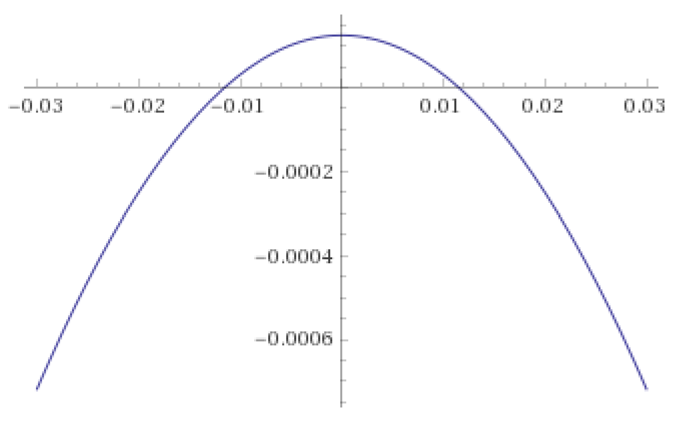

$$H_z = \frac{M_z}{4\pi R^3}\left(1 - \frac{3z^2}{R^2})(1 + kR) + (1 - \frac{z^2}{R^2})k^2R^2\right)e^{-kR}$$

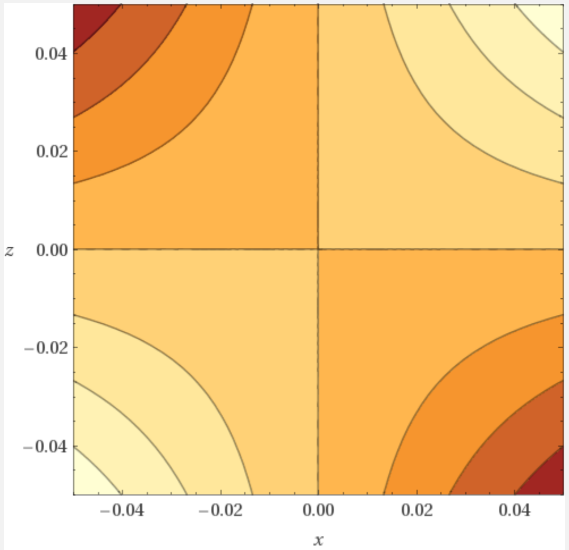

$$k^2 = -i\omega\mu\sigma\text{-}\omega^2\mu\sigma$$

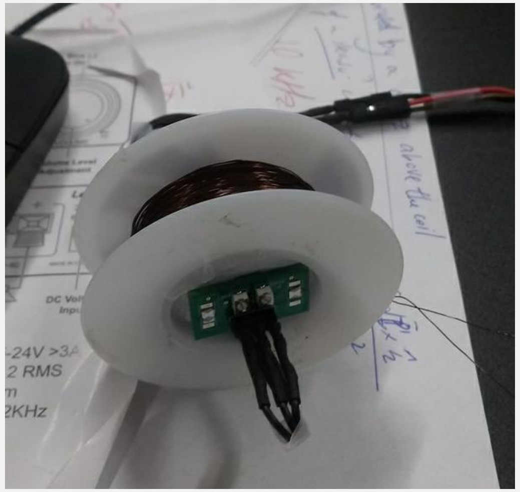

$$H_x = \frac{M_z xz}{4\pi R^5}(3 + 3kR + k^2R^2)e^{-kR}$$

Fig. 13. Field of the small coil

Attempts to detect a hole

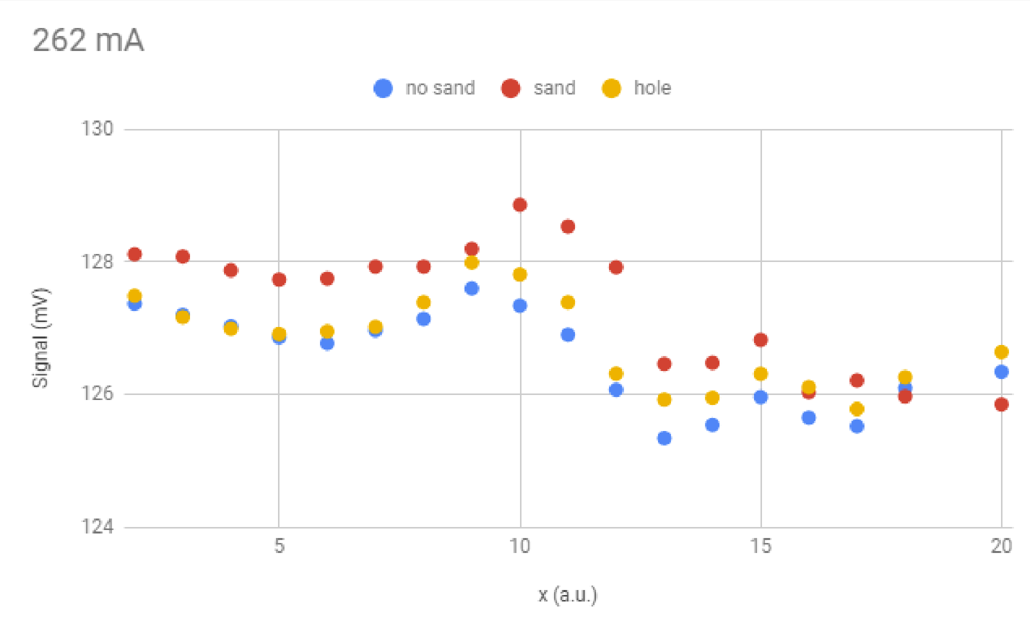

Fig. 14. First measurements

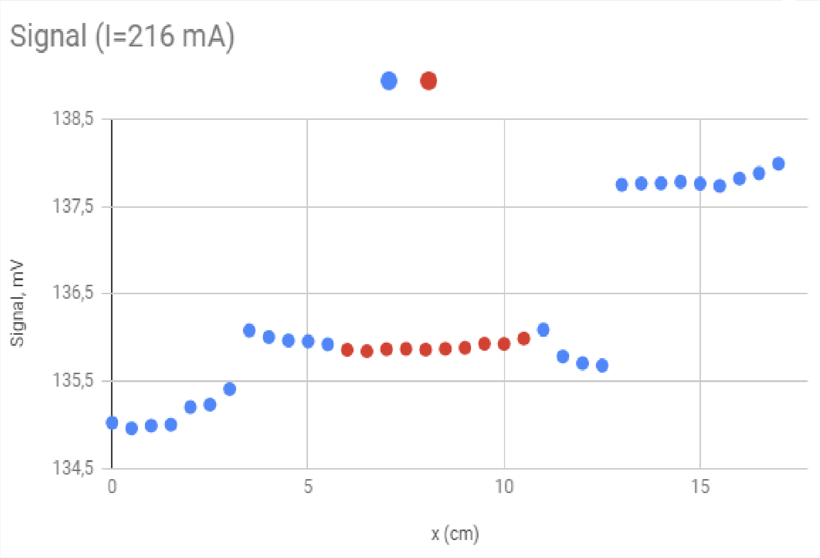

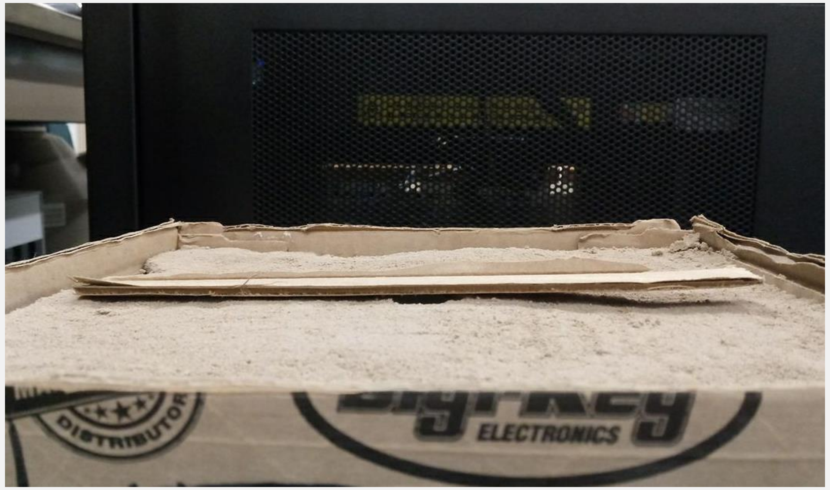

Fig. 15. Second measurement

Directions for the future work

- Get consistent reading
- Observe the signal from the coil (expand the field range of MTJ)
- Optimize the iron powder and magnetic sand parameters
- Optimize the choice of the coil winding and power consumption
- Push the detectability limit (currently the hole diameter is around 1 cm)
- Perform 3D simulation
- Move to the cylindrical model

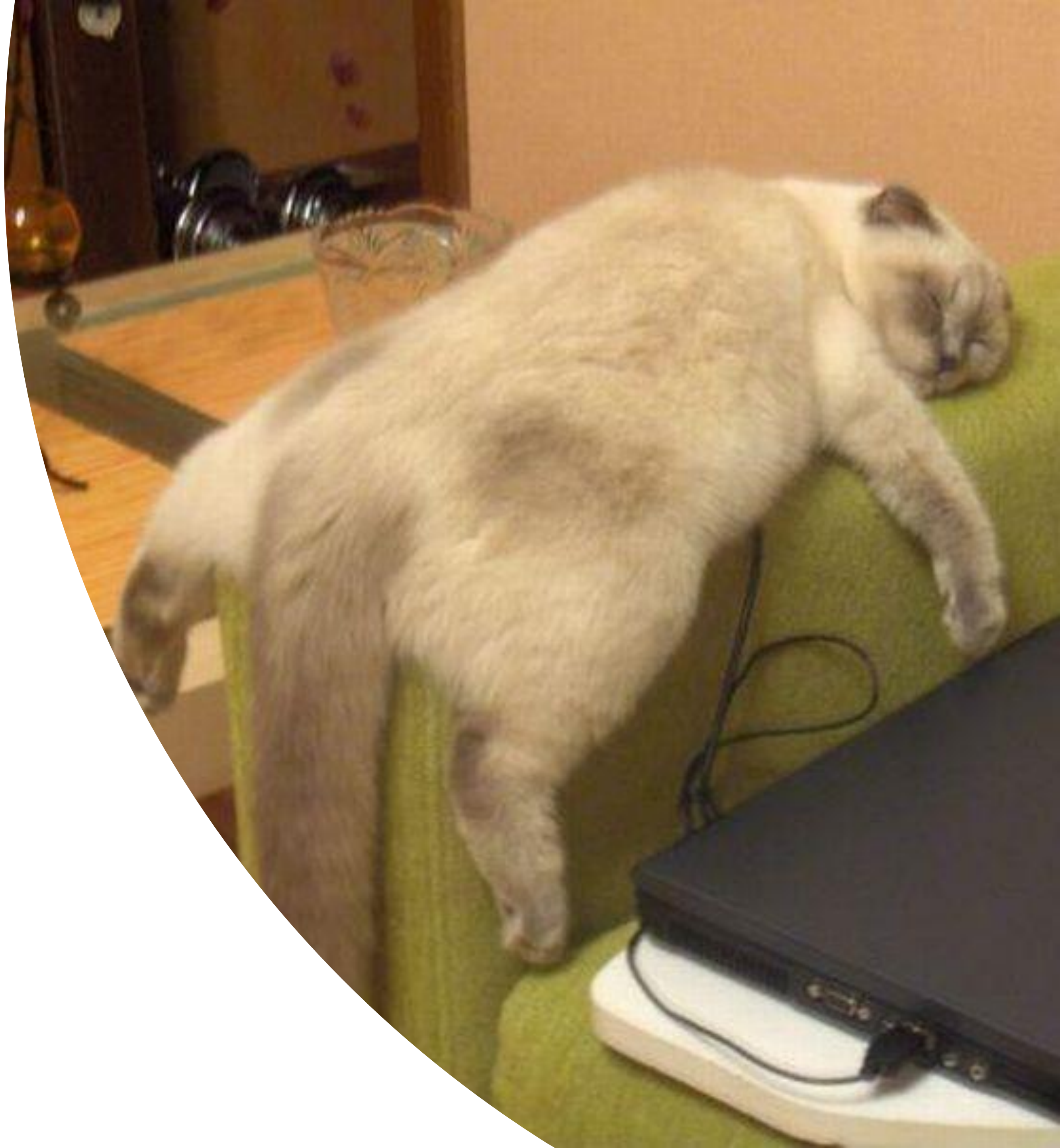

Acknowledgements

- Prof. Gang Xiao, Physics Department of Brown University
- He Guanyang, Zhang Yiou (Physics Department of Brown University), Timofey Eltsov (KAUST)
- Physics Department of Brown University
- Physics Department of The Chinese University of Hong Kong

- Wu Yee Sun College
- Global Internship Programme

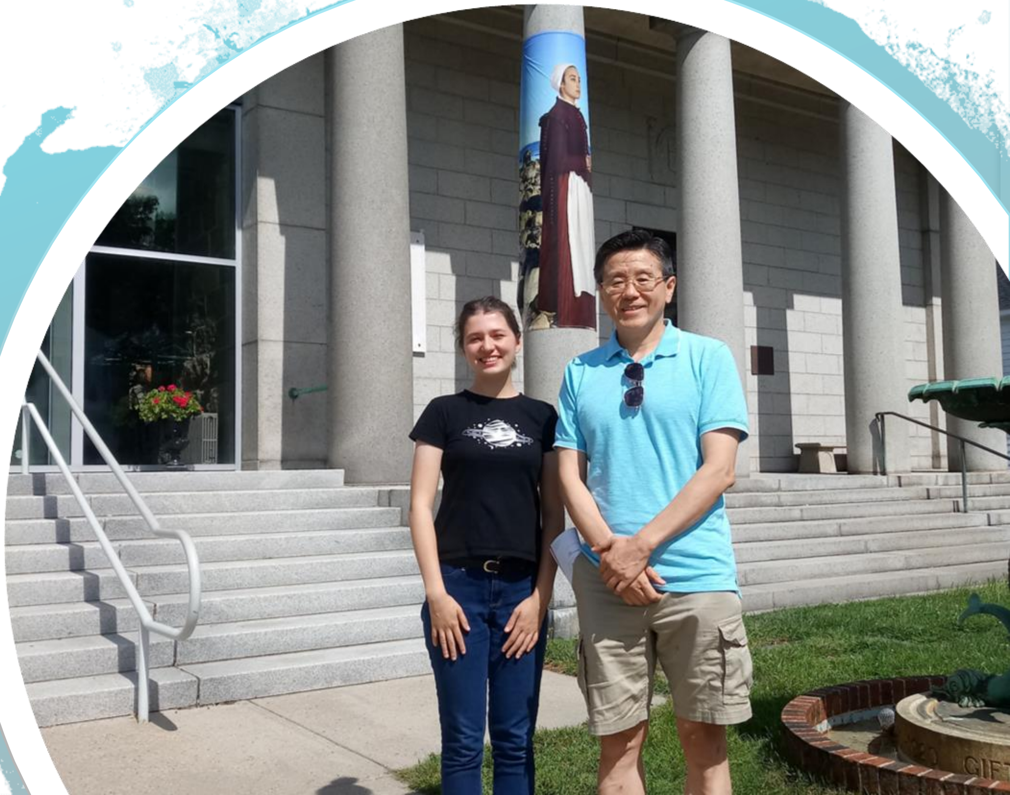

Thank you!

References

- “Handbook of Spin Transport and Magnetism”, edited by Evgeny Y. Tsymbal, Igor Zutic. “Magnetoresistive Sensors Based on Magnetic Tunneling Junctions”, Gang Xiao
- SPE Middle East Oil and Gas Show and Conference 2019 “Beyond Steel Casing: Detecting Zonal Isolation in the Borehole Environment”, T. Eltsov, T. W. Patzek
- “PicoTesla Magnetic Sensors based on Magnetic Tunneling Junctions with Double-staged Flux Concentrators”, G. He, Y. Zhang, L. Qian, G. Xiao, - APS Meeting Abstracts, 2019